

Spin-wave stiffness in the Dzyaloshinskii-Moriya helimagnets $\text{Mn}_{1-x}\text{Fe}_x\text{Si}$

S. V. Grigoriev,^{1,2,3} E. V. Altyntbaev,^{1,2,3} S.-A. Siegfried,⁴ K. A. Pschenichnyi,^{1,2,3} D. Menzel,⁵
A. Heinemann,⁴ and G. Chaboussant⁶

¹*Petersburg Nuclear Physics Institute NRC “Kurchatov institute”, Gatchina, St-Petersburg, 188300, Russia*


²*Saint-Petersburg State University, Ulyanovskaya 1, Saint-Petersburg, 198504, Russia*

³*Institute for High Pressure Physics, Russian Academy of Sciences, 142190 Troitsk, Moscow, Russia*

⁴*Helmholtz Zentrum Geesthacht, Geesthacht, 21502, Germany*

⁵*Technische Universität Braunschweig, 38106 Braunschweig, Germany*

⁶*Laboratoire Leon Brillouin, CEA Saclay, 91191 Gif-sur-Yvette Cedex, France*

 (Received 11 August 2017; revised manuscript received 1 November 2017; published 9 January 2018)

The small-angle neutron scattering is used to measure the spin-wave stiffness in the field-polarized state of the Dzyaloshinskii-Moriya helimagnets $\text{Mn}_{1-x}\text{Fe}_x\text{Si}$ with $x = 0.03, 0.06, 0.09,$ and 0.10 . The $\text{Mn}_{1-x}\text{Fe}_x\text{Si}$ compounds are helically ordered below T_c and show a helical fluctuation regime above T_c in a wide range up to T_{DM} . The critical temperatures T_c and T_{DM} decrease with x and tend to 0 at $x = 0.11$ and 0.17 , respectively. We have found that the spin-wave stiffness A change weakly with temperature for each individual Fe-doped compound. On the other hand, the spin-wave stiffness A decreases with x duplicating the T_{DM} dependence on x , rather than $T_c(x)$. These findings classify the thermal phase transition in all $\text{Mn}_{1-x}\text{Fe}_x\text{Si}$ compounds as an abrupt change in the spin state caused, most probably, by the features of an electronic band structure. Moreover, the criticality in these compounds is not related to the value of the ferromagnetic interaction but demonstrates the remarkable role of the Dzyaloshinskii-Moriya interaction as a factor destabilizing the magnetic order.

DOI: [10.1103/PhysRevB.97.024409](https://doi.org/10.1103/PhysRevB.97.024409)

I. INTRODUCTION

The energy landscape of the magnetic systems determines both the resultant magnetic structure and magnetic excitations. This is clearly demonstrated for the cubic B20-type compounds with the Dzyaloshinskii-Moriya (DM) interaction. The competition between the ferromagnetic exchange interaction and the antisymmetric DM interaction leads to the appearance of the homochiral helical magnetic structure [1,2]. Moreover the magnetic field-temperature (H - T) phase diagram replicates itself in all these compounds showing transitions first from the plain spiral to the conical state and then to the fully polarized state upon enhancement of the field. Another feature of the (H - T) phase diagram is the appearance of a skyrmion lattice in the narrow range of the magnetic fields close to the critical temperature T_c . The skyrmion lattice and its position in the (H - T) phase diagram may be considered as a fingerprint of the magnetic interactions inherent to the B20-type compounds.

Similarly, the spin-wave excitations are directly determined by the same set of the magnetic interactions. The theory predicts a highly anisotropic spin-wave spectrum with a linear dispersion at $\mathbf{q} \parallel \mathbf{k}_s$ and quadratic one at $\mathbf{q} \perp \mathbf{k}_s$ for the long-wave excitations ($q < k_s$) where k_s is the wave vector of the helix [3–5]. Another remarkable feature of the helimagnon spectrum is its intrinsic multimode nature caused by the periodic potential of the helical structure [6,7]. Moreover, even in the fully polarized state the spin waves are strongly anisotropic. The spin-wave energy in this case was explicitly given by Kataoka in [4]

$$\epsilon_{\mathbf{q}} = A(\mathbf{q} - \mathbf{k}_s)^2 + (H - H_{C2}), \quad (1)$$

where \mathbf{k}_s matches with the orientation of the external magnetic field. The sign of the DM constant determines the direction of the helix wave-vector k_s being parallel or antiparallel with respect to the direction of the field. Here and further on we omit the factor $g\mu_B$ at the value of the field H for simplicity but imply H is measured in the energy units.

The validity of the spin-wave dispersion [Eq. (1)] has recently been experimentally proven using the small-angle polarized neutron scattering [8]. Using polarized neutrons it was demonstrated that the sign of the DM constant determines a preferable clockwise or anticlockwise rotation of the spin waves, i.e., the chirality of the DM helimagnets results in one-handed excitations in the full-polarized state. The analysis of the scattering patterns allows one to measure the spin-wave stiffness as a function of the temperature. Conclusions derived in [8] on the basis of SANS measurements have been proven once again using triple-axis spectroscopy [9]. The complementarity of the two methods have been clearly discussed in [8].

It can be analytically shown that the inelastic neutron scattering in the case of DM helimagnets is concentrated mostly around the momentum transfers corresponding to $\pm \mathbf{k}_s$ within two narrow cones limited by the cut-off angle θ_C for the energy gain/energy loss, respectively [8]. The cut-off angle θ_C is connected to the spin-wave stiffness A via the dimensionless parameter $\theta_0 = \hbar^2/(2Am_n)$:

$$\theta_C^2(H) = \theta_0^2 - \frac{\theta_0}{E_i}H + \theta_B^2, \quad (2)$$

where m_n is the neutron mass, θ_B is the Bragg angle of the scattering on spin spiral with the length $2\pi/k_s$, and E_i denotes the energy of incident neutrons.

It is also known that the substitution of manganese by iron in the isostructural solid solutions $\text{Mn}_{1-x}\text{Fe}_x\text{Si}$ suppresses the helical spin state [10]. The neutron scattering studies [11,12] together with magnetic data and specific heat measurements [10,13,14] discovered a quantum critical point (QCP) corresponding to the suppression of the spin spiral phase with long-range order (LRO) in $\text{Mn}_{1-x}\text{Fe}_x\text{Si}$. This QCP located at $x_{c1} \approx 0.11-0.12$ is, however, hidden by a spin helix fluctuation [12–14]. This spin helix fluctuation regime, sometimes referred to as chiral spin liquid [15,16], vanishes at the second QCP $x_{c2} \approx 0.24$. Thus it has been shown that $\text{Mn}_{1-x}\text{Fe}_x\text{Si}$ undergoes a sequence of the two quantum phase transitions [14]. A close look at the Hall effect data in $\text{Mn}_{1-x}\text{Fe}_x\text{Si}$ had shown that the substitution of Mn with Fe results rather in hole doping opposite to naturally expected electron doping [17]. The two groups of the charge carriers contribute to the Hall effect and the ratio between them changes the sign of the Hall effect constant at $x_{c1} \approx 0.11$, what is definitely associated with the QCP in these compounds.

In spite of numerous studies of the spin-wave dynamics in MnSi [6–9,18–20], there were no attempts to perform measurements on the spin-wave dynamics of the doped compounds such as $\text{Mn}_{1-x}\text{Fe}_x\text{Si}$, $\text{Fe}_{1-x}\text{Co}_x\text{Si}$, etc. In this paper we report on the direct measurements of the spin-wave stiffness of the several representatives of $\text{Mn}_{1-x}\text{Fe}_x\text{Si}$ using a small-angle neutron scattering technique. As the major experimental achievement, we demonstrate that the magnetic system of these compounds shows little softening with temperature T while it does with increase of the dopant concentration x .

II. EXPERIMENT

The series of $\text{Mn}_{1-x}\text{Fe}_x\text{Si}$ single crystals with $x = 0.03, 0.06, 0.09$, and 0.108 were grown using the Czochralski technique. These samples were prepared as cylinders with a height of 8–10 mm and a diameter of 3–4 mm. Magnetic measurements of the newly synthesized compounds were carried out with a Quantum Design MPMS-5S SQUID-magnetometer, which is located at the Institute of Condensed Matter Physics, TU Braunschweig, Germany. The temperature dependencies of the susceptibility χ in the magnetic field $H = 10$ mT are shown in Fig. 1 for the $\text{Mn}_{1-x}\text{Fe}_x\text{Si}$ compounds with $x = 0, 0.03, 0.06$, and 0.09 . The corresponding curves for the sample with $x = 0.108$ is given in [21].

The experiments with the doped $\text{Mn}_{1-x}\text{Fe}_x\text{Si}$ compounds should be placed within the context of earlier studies of the phase transition in pure MnSi. As was demonstrated in [12,22,23], there are two characteristic temperatures which determine a transition from disordered to the helical state: namely, a transition into the helix phase at T_c (LRO transition) and a crossover to the helix fluctuating regime at T_{DM} (SRO crossover). These critical temperatures (T_c and T_{DM}) have been determined as a maximum and a minimum of the derivative of the susceptibility with respect to the temperature $d\chi/dT$ in accord with the approach used in [12]. The derivative of the susceptibility on temperature $d\chi/dT$ for the compound with $x = 0.03$ is shown as an example in the inset of Fig. 1. These inflection points divide the temperature scale into the three regions: (i) the helix phase (LRO) occurs from low temperatures to T_c (maximum of $d\chi/dT$); (ii) the fluctuating

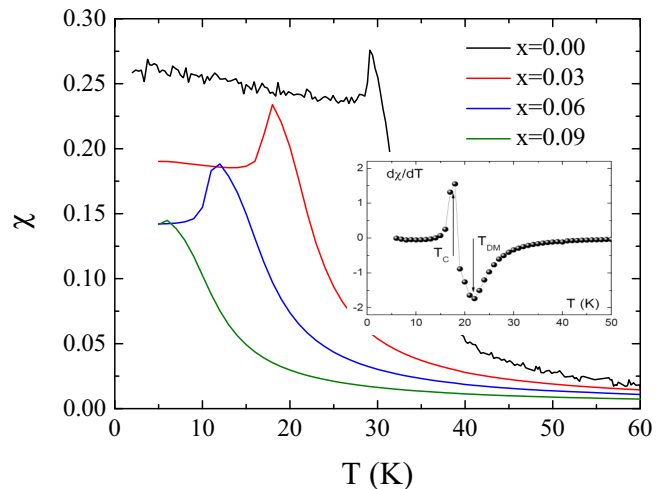


FIG. 1. The temperature dependencies χ in the magnetic field $H = 10$ mT for the $\text{Mn}_{1-x}\text{Fe}_x\text{Si}$ compounds with $x = 0, 0.03, 0.06$, and 0.09 . The inset shows a temperature derivative of the susceptibility $d\chi/dT$ for sample with $x = 0.03$. The definitions of T_c and T_{DM} are given in the text.

helical regime occupies a band between T_c and T_{DM} (minimum of $d\chi/dT$); and (iii) the paramagnetic phase is identified above T_{DM} . The crossover temperature T_{DM} denotes the point of the change of the character of the spin fluctuations from a helical (i.e., with DM interaction) to a ferromagnetic one (i.e., where DM interaction can be neglected).

Thus, it is well established that the transition is based on a smooth temperature evolution of the spin fluctuations into the helix structure [22–24]. An interplay of two length scales—the spiral period d_s and the correlation length of the critical fluctuations ξ —results in the appearance of new magnetic properties in the system upon temperature decrease. The concept proposed in [24] and developed in [22,23] starts with the short range correlations at high temperature ($\xi \ll d_s$). This high-temperature range can be well described by the ferromagnetic type of the fluctuations, when the Dzyaloshinskii-Moriya (DM) interaction is neglected. When the correlation length ξ approaches the value of d_s , the ferromagnetic description of the spiral fluctuations is no more applicable. The DM interaction becomes noticeable and the full scale (“true”) helix fluctuations can be realized when ξ becomes larger than d_s . The crossover from ferromagneticlike regime to helixlike regime of fluctuations occurs at $T_{DM} = 32.5$ K, when $\xi \approx d_s$. It was shown in [22] that the system may undergo another crossover to the regime of the anisotropic fluctuations at $T_A < T_{DM}$. The magnetic system transforms finally into the steady spiral at $T_c = 29$ K. The transition should be of the second order, if one takes into account the anisotropy of fluctuations. These three regimes were named in [23] as Bak-Jensen regime, Brazovskii regime [25], and Wilson-Fisher regime, respectively. If one suggests that the anisotropy is weak, then the phase transition becomes the fluctuation-induced first-order one with two characteristic temperatures T_{DM} and T_c [23].

The temperature-concentration ($T-x$) phase diagram is shown in Fig. 2. It is apparent in Fig. 2 (in accord with [12–14,17]) that T_c approaches 0 at $x_c \approx 0.11-0.12$, while

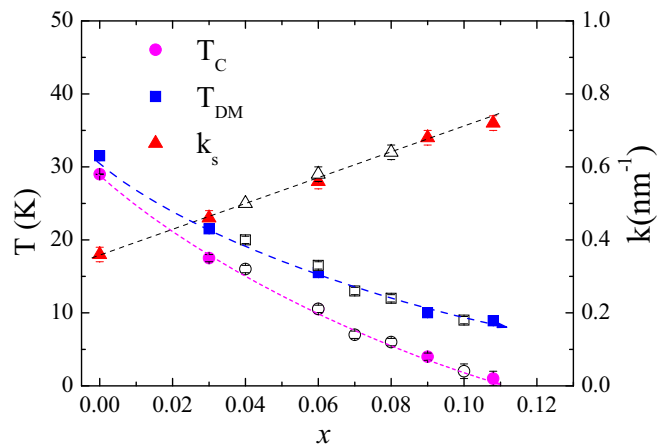


FIG. 2. Temperature-concentration (T - x) phase diagram of the $\text{Mn}_{1-x}\text{Fe}_x\text{Si}$ compounds. The helix wave vector k as a function of x . Closed symbols give values for the samples of present study. The open symbols are taken from [11,12] with the systematic shift $\delta x = -0.02$. The dashed lines are guides for the eye.

the band of the fluctuating helix regime increases with x . The decrease of T_c is accompanied by the linear with x increase of the helix wave vector k , as shown in Fig. 2. Comparing the data presented in this paper with those of the papers [11,12] one should note the discrepancy between them. It appears that the set of samples in [11,12] grown by the Bridgman method have the systematic shift in the concentration x roughly equaled to $+0.02$ as compared to the samples used in the given study produced by the Czochralski method. We added the experimental points of [11,12] to Fig. 2, however, shifted for -0.02 along the x axis. It is seen that dependencies of k , T_{DM} , and T_c taken from different sets of the samples match each other. Such a shift in no way harms the conclusions of [11,12], or the results discussed below.

Following the protocol of measurements given in [8], we have determined the spin-wave stiffness in the fully polarized state for the $\text{Mn}_{1-x}\text{Fe}_x\text{Si}$ compounds using small-angle neutron scattering. The polarized and nonpolarized small-angle neutron scattering were performed for the single crystals with $x = 0.03, 0.06$, and 0.09 using the PA20 instrument ($\lambda = 0.51$ nm) at the Orphei reactor at the LLB (France) and for the single crystal with $x = 0.108$ using the SANS-1 instrument ($\lambda = 0.5$ nm) at the FRM-II reactor at the MLZ (Germany). A magnetic field up to 5 T was applied along Q_y perpendicular to the neutron beam. The [110] axis of the single crystals was oriented parallel to the applied field with accuracy of 5° . Background intensity maps were taken for all samples at low temperature ($T = 5$ K) and high magnetic field ($H = 5$ T) when both the elastic magnetic peak and spin-wave scattering are fully suppressed. These background maps were subtracted from the other scattering maps of the given sample. We used the data-reduction software GRASP developed at the ILL, Grenoble [26].

III. RESULTS

Figure 3 shows typical SANS maps exhibiting the spin-wave scattering for the sample with $x = 0.03$ taken at the

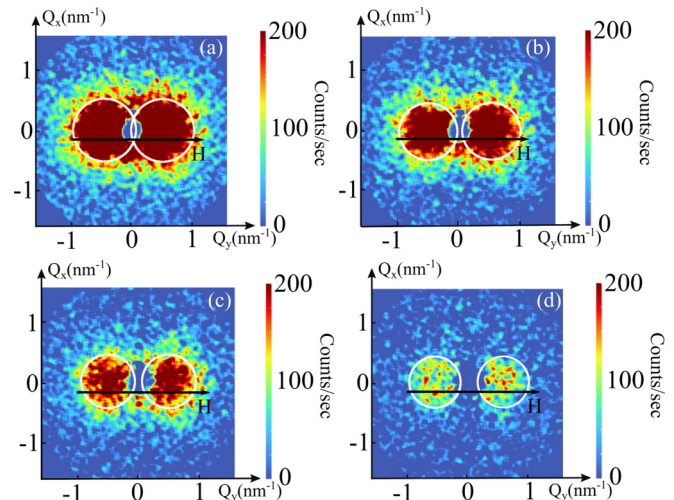


FIG. 3. Maps of the SANS intensities for the single crystal $\text{Mn}_{1-x}\text{Fe}_x\text{Si}$ with $x = 0.03$ taken at $T = 10$ K at the field above H_{c2} (a) $H = 0.7$ T, (b) $H = 0.9$ T, (c) $H = 1.1$ T, and (d) $H = 1.8$ T. The arrows show the direction of the field.

different fields above H_{c2} at $T = 10$ K, i.e., below $T_c = 17$ K. These scattering patterns appear as two round spots centered at the wave vector positions $\pm \mathbf{k}$ directed along the applied magnetic field. The size of these spots shrinks remarkably with the field, being limited by the value $Q_c = k_n \theta_C$, where θ_C is the cut-off angle related to the spin-wave stiffness [Figs. 3(a)–3(d)].

The evolution of a scattering pattern with the field is not trivial and is worthy of discussion. As the field exceeds $H_{c2} \approx 0.6$ T, the elastic magnetic peak disappears and only the inelastic scattering centered at $\mathbf{Q} = \pm \mathbf{k}_s$ remains. This scattering intensity consists of two contributions: the strong diffuse part in the vicinity of the former magnetic peak at $\mathbf{Q} = \pm \mathbf{k}_s$ and the round spot limited by the critical angle θ_C . The diffuse contribution is maximal at $H \approx H_{c2}$ and is strongly suppressed by further increase of the field: $I(\theta = \theta_B) \sim I_0 / (H - H_{c2})$ (see inset in Fig. 4). The round spots caused by the spin-wave scattering are less affected by the magnetic field. According to Eq. (2) the spin-wave part of the scattering becomes narrower with increase of the field and should vanish at a certain H_{off} well above H_{c2} . Using Eq. (2), we define this value as $H_{\text{off}} = \theta_0 E_i$.

To improve the statistics, the scattering intensity of the SANS maps was azimuthally averaged over the angular sector of 120 deg with the center positioned at $\mathbf{Q} = \pm \mathbf{k}_s$. An example of the profile transformation with the field is shown in Fig. 4.

The measured intensity can be fitted by the product of a sigmoid function and a Lorentz function, which captures the main features of the scattering:

$$I(\theta) = \frac{I_0}{(\theta - \theta_B)^2 + \kappa^2} \left\{ \frac{1}{2} - \left(\frac{1}{\pi} \arctan \left[\frac{2(\theta - \theta_C)}{\delta} \right] \right) \right\}. \quad (3)$$

Here the Lorentz function describes the contribution of the diffuse scattering and its parameter $\kappa^2 \approx (\theta_0 / E_i)(H - H_{c2})$ reflects the closeness of the system to the critical field H_{c2} . The sigmoid serves as a steplike function with cut-off angle

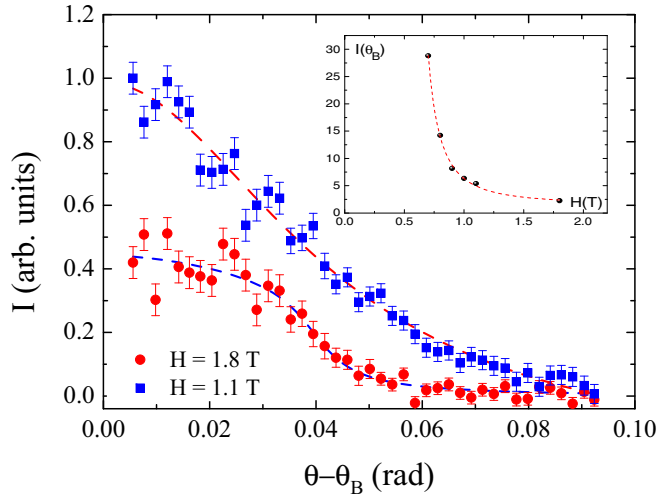


FIG. 4. The radially averaged scattering intensity centered at the Bragg peak position I vs scattered angle $\theta - \theta_B$ for the single crystal $\text{Mn}_{1-x}\text{Fe}_x\text{Si}$ with $x = 0.03$ taken at $T = 10$ K and at $H = 1.1$ T and $H = 1.8$ T. The broken lines are the results of the fit using Eq. (3). The inset shows the field dependence of the scattering intensity at the Bragg position $I(\theta_B)$ at $H > H_{c2}$.

θ_C , which is smeared over by its width δ . It is related to the spin-wave damping as $\Gamma \approx \delta E_i$.

A sharp cutoff of the intensity was not observed for any measured field due both large contribution of the diffuse scattering and/or the spin-wave damping. Nevertheless the application of the field that is strong enough to suppress the diffuse scattering (case of $H = 1.8$ T in Fig. 4) allows one to clearly determine the cut-off angle θ_C .

Figure 5 shows typical SANS maps of the spin-wave scattering for the sample with $x = 0.03$ taken at different temperatures in the field $H = 1.8$ T, i.e., when the diffuse scattering is practically suppressed. The position and size of

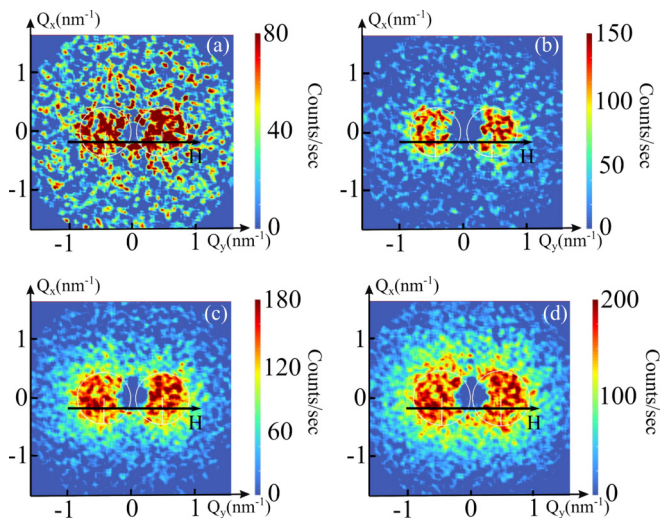


FIG. 5. Maps of the SANS intensities for the single crystal $\text{Mn}_{1-x}\text{Fe}_x\text{Si}$ with $x = 0.03$ taken at the field 1.8 T and (a) $T = 4$ K, (b) $T = 10$ K, (c) $T = 15$ K, and (d) $T = 17$ K. The arrows show a field direction.

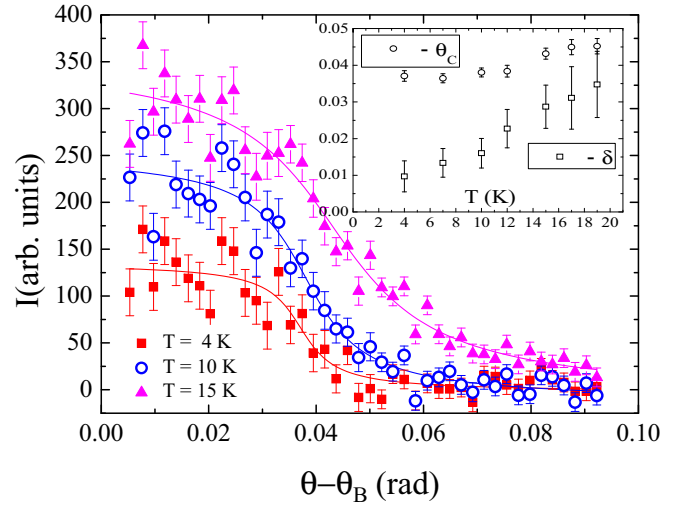


FIG. 6. The radially averaged scattering intensity $I(\theta - \theta_B)$ for the single crystal $\text{Mn}_{1-x}\text{Fe}_x\text{Si}$ with $x = 0.03$ taken at the field 1.8 T and $T = 4, 10,$ and 15 K. The solid lines are the results of the fit using Eq. (3). The inset shows temperature dependencies of the cut-off angle θ_C and the width δ obtained from the fit to data at $H = 1.8$ T.

the spots change little with the temperature, as one can see from Figs. 5(a)–5(d). The radially averaged scattering intensity I as a function of the scattered angle $\theta - \theta_B$ at different temperatures and $H = 1.8$ T is shown in Fig. 6. The intensity profile at low temperature ($T = 4$ K) is well reproduced by the steplike function with an abrupt step. Although it is smeared by the resolution function and contaminated by poor statistics. The smearing of a step becomes noticeable with temperature increase. Moreover, the width of smearing δ is comparable to the cut-off angle θ_C in a high-temperature range, close and above T_c , where the magnetic system enters the critical regime ruled by the thermal fluctuations. Thus, we describe all sets of data using the spin-wave concept based on a low-temperature approximation. Nevertheless, the spin-wave concept can be applied to the system close to T_c subjected to the strong magnetic field, which suppresses critical fluctuations.

The experimental data were fitted by the expression given by Eq. (3). The cut-off angle θ_C and the width δ were extracted from the fit and plotted as a function of temperature as inset in Fig. 6. The following three facts are worthy to be noted: First, the spin-wave stiffness can be determined even above T_c up to T_{DM} since the magnetic system can be polarized in this temperature range. Although the value of the cut-off angle θ_0 is comparable to the the smearing width δ in the vicinity of T_c . Second, it stays practically constant at low temperatures as well as in the critical range. Third, the spin waves experience damping, which increases linearly with temperature $\Gamma \sim T$. The mechanism of the spin-wave damping remains unclear.

In the similar way taken and treated data for the compound with $x = 0.108$ are shown in Figs. 7 and 8. The maps of the scattering intensities taken at field 1.8 T and temperature $T = 3, 5,$ and 7 K are shown in Figs. 7(a)–7(c), respectively. Although all these maps were taken at temperatures above $T_c \approx 1$ K, the detected scattering intensity concentrated in the vicinity of $\mathbf{Q} = \pm \mathbf{k}_s$ is limited by the critical angle θ_C . The

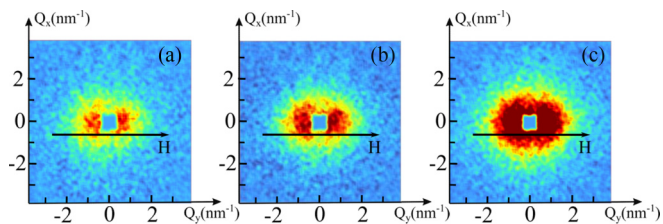


FIG. 7. Maps of the SANS intensities for the single crystal $\text{Mn}_{1-x}\text{Fe}_x\text{Si}$ with $x = 0.108$ taken at the field 1.8 T and (a) $T = 3$ K, (b) $T = 5$ K, and (c) $T = 7$ K. The arrows show a field direction.

radially averaged scattering intensity I vs $\theta - \theta_B$, given in Fig. 8, is well fitted by the steplike function of Eq. (3).

Using Eq. (2) one can determine the value of θ_0 and the spin-wave stiffness A . The temperature dependence of the spin-wave stiffness obtained from the detection of the cut-off angle of the different compounds is presented in Fig. 9. We observe a weak dependence of the spin-wave stiffness A with temperature and the finite values of A at T_c for the compounds under study. For completeness we added the temperature dependence of the stiffness A for the pure MnSi measured by the same method as in [8]. In order to extrapolate the measured values of the stiffness to $T = 0$, the temperature dependencies $A(T)$ for all compounds were fitted by the power law: $A(T) = A_0[1 - c(T/T_c)^z]$ with the fixed index $z = 5/2$, as it can be expected for the ferromagnets. The value of z has little influence on the parameter A_0 since the temperature dependence of A is weak. It could be expected for second-order transition that the spin waves soften near T_c , what is not observed. In opposite, the phase transition in all $\text{Mn}_{1-x}\text{Fe}_x\text{Si}$ compounds can be classified as an abrupt change in the spin state caused, most probably, by the features of an electronic band structure [27,28].

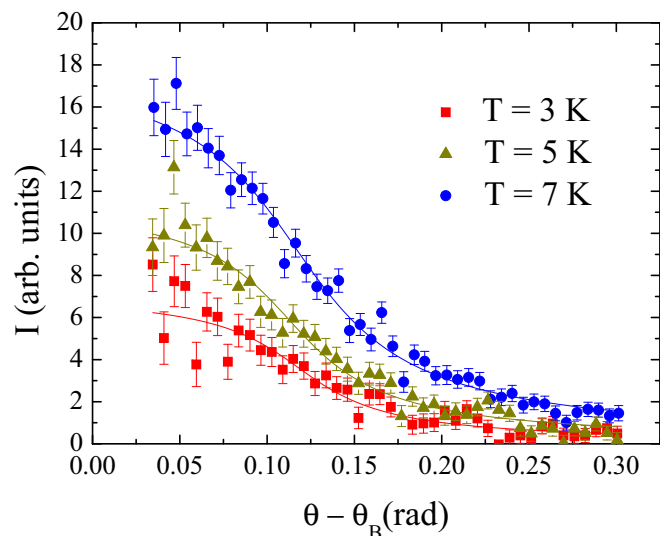


FIG. 8. The radially averaged scattering intensity $I(\theta - \theta_B)$ for the single crystal $\text{Mn}_{1-x}\text{Fe}_x\text{Si}$ with $x = 0.108$ taken at the field 1.8 T and $T = 3, 5,$ and 7 K. The solid lines are the results of the fit using Eq. (3).

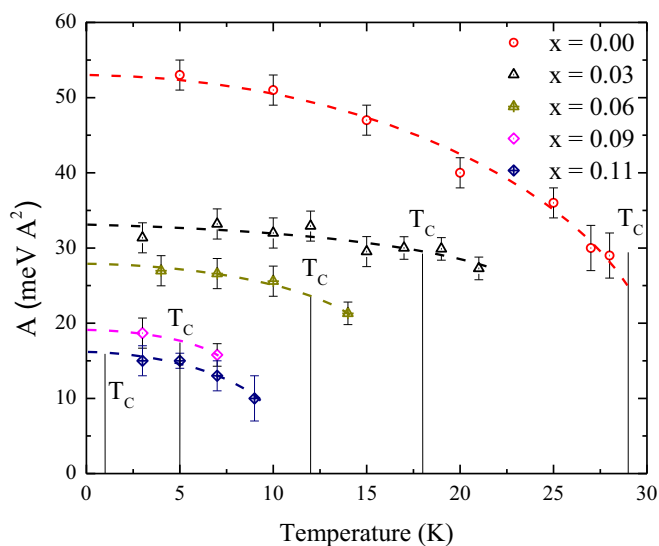


FIG. 9. Temperature dependence of the spin-wave stiffness A . Dashed lines are fits to a power law (see text).

Although the value of A changes little with temperature, it apparently decreases remarkably from one sample to another, i.e., with increase of x . In order to reveal the link between the spin-wave stiffness and the critical temperatures, we plotted A_0 for the different $\text{Mn}_{1-x}\text{Fe}_x\text{Si}$ compounds against the characteristic temperatures T_c and T_{DM} in Fig. 10. As seen from the plot, the spin-wave stiffness is linearly proportional to T_c for small x and to T_{DM} for the compounds with large x , i.e., close to the QCP. This observation implies that the long range helical order limited by T_c is determined by the isotropic exchange A for pure MnSi and compounds with small doping concentration $x < 0.05$. The phase transition in these compounds is well described by the concept developed for pure MnSi in [22–24]. As to the compounds with large x , i.e., close to the QCP, the long range helical order is additionally destabilized by another mechanism. This additional source of

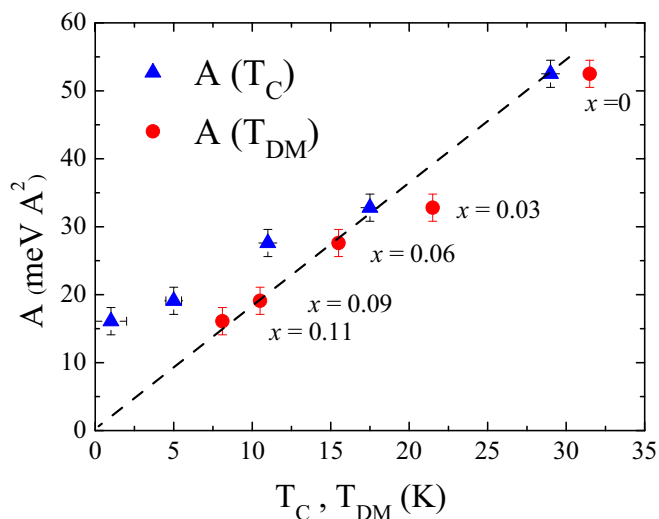


FIG. 10. The spin-wave stiffness A of the $\text{Mn}_{1-x}\text{Fe}_x\text{Si}$ compounds versus the characteristic temperatures T_c and T_{DM} .

the instability can naturally be the DM interaction, the strength of which can be roughly estimated via the helix wave vector k_s .

Recently the influence of spin fluctuations on the thermodynamic properties the pure MnSi has been investigated in the framework of the Hubbard model with the electronic spectrum determined from the first-principles LDA + U + SO calculation, which was extended taking into account the Hund coupling and the Dzyaloshinskii Moriya antisymmetric exchange [27,28]. Going beyond the Brazovskii model [25], it has been shown that the ground state of the magnetic material is characterized by large zero-point fluctuations. The evaluations showed that the total amplitude of zero-point and thermal spin fluctuations is large compared with the amplitude of the magnetization and varies little in a fairly wide temperature range. They disappear in the vicinity of T_c only. In this case, the entropy abruptly increases, causing thermal fluctuations which, in turn, lead to the disappearance of the local moment. A competition between the increase in entropy due to paramagnon excitations and its decrease as a result of the reduction in the amplitude of local magnetic moments, under the conditions of strong Hund exchange, is responsible for in the appearance of the peculiar critical phenomena observed in MnSi. Among these phenomena are an anomalous sharp lambda-shaped maxima and minima in the temperature dependencies of the heat capacity and thermal expansion coefficient of the MnSi ferromagnet [29,30].

Thus, the first-principles calculations [27,28] demonstrate that coupling between the electronic structure and the spin state can explain, first, the magnetic state of MnSi with two characteristic features near the transition temperature that are related to the suppression of magnetic moments of the

helical ferromagnetic state at T_{DM} and the vanishing of helical ordering at T_c . Second, these calculations explain stability of the magnetic state in a wide range and its abrupt change at T_c .

As was noted in [28], these calculations can be applied to the $Mn_{1-x}Fe_xSi$ compounds as soon as the chemical potential level is located in the region of energies of nondegenerate orbital states although their electronic structure requires further investigation. In view of the concept discussed above an intriguing question remains unsolved: Are the fluctuations $Mn_{1-x}Fe_xSi$ compounds of a quantum or thermal nature? How can they be distinguished experimentally? These questions are to be answered in the forthcoming studies.

IV. CONCLUSION

In conclusion, we have experimentally determined the spin-wave stiffness in the $Mn_{1-x}Fe_xSi$ compounds. We have found that the spin-wave stiffness A for the Fe-doped compounds is weakly dependent on temperature. This finding shows that the criticality at T_c is not related to the value of the ferromagnetic interaction but is significantly modified by the Dzyaloshinskii-Moriya interaction. The spin-wave stiffness A decreases with x duplicating the T_{DM} dependence on x , rather than $T_c(x)$. This points out the remarkable role of the Dzyaloshinskii-Moriya interaction as the destabilizing factor for the magnetic order in these compounds.

ACKNOWLEDGMENTS

The authors thank A. A. Povzner and T. A. Nogovitsyna for fruitful discussions. They are grateful for the support of the Russian Science Foundation (Grant No. 17-12-01050).

-
- [1] O. Nakanishia, A. Yanase, A. Hasegawa, and M. Kataoka, *Solid State Commun.* **35**, 995 (1980).
 - [2] P. Bak and M. H. Jensen, *J. Phys. C* **13**, L881 (1980).
 - [3] S. V. Maleyev, *Phys. Rev. B* **73**, 174402 (2006).
 - [4] M. Kataoka, *J. Phys. Soc. Jpn.* **56**, 3635 (1987).
 - [5] D. Belitz, T. R. Kirkpatrick, and A. Rosch, *Phys. Rev. B* **73**, 054431 (2006).
 - [6] M. Janoschek, F. Bernlochner, S. Dunsiger, C. Pfleiderer, P. Boni, B. Roessli, P. Link, and A. Rosch, *Phys. Rev. B* **81**, 214436 (2010).
 - [7] M. Kugler, G. Brandl, J. Waizner, M. Janoschek, R. Georgii, A. Bauer, K. Seemann, A. Rosch, C. Pfleiderer, P. Böni, and M. Garst, *Phys. Rev. Lett.* **115**, 097203 (2015).
 - [8] S. V. Grigoriev, A. S. Sukhanov, E. V. Altyntbaev, S.-A. Siegfried, A. Heinemann, P. Kizhe, and S. V. Maleyev, *Phys. Rev. B* **92**, 220415(R) (2015).
 - [9] H. Tran and N. E. Bonesteel, *Phys. Rev. B* **84**, 144420 (2011).
 - [10] Y. Nishihara, S. Waki, and S. Ogawa, *Phys. Rev. B* **30**, 32 (1984).
 - [11] S. V. Grigoriev, V. A. Dyadkin, E. V. Moskvina, D. Lamago, Th. Wolf, H. Eckerlebe, and S. V. Maleyev, *Phys. Rev. B* **79**, 144417 (2009).
 - [12] S. V. Grigoriev, E. V. Moskvina, V. A. Dyadkin, D. Lamago, T. Wolf, H. Eckerlebe, and S. V. Maleyev, *Phys. Rev. B* **83**, 224411 (2011).
 - [13] A. Bauer, A. Neubauer, C. Franz, W. Munzer, M. Garst, and C. Pfleiderer, *Phys. Rev. B* **82**, 064404 (2010).
 - [14] S. V. Demishev, I. I. Lobanova, V. V. Glushkov, T. V. Ishchenko, N. E. Sluchanko, V. A. Dyadkin, N. M. Potapova, and S. V. Grigoriev, *JETP Lett.* **98**, 829 (2014).
 - [15] S. Tewari, D. Belitz, and T. R. Kirkpatrick, *Phys. Rev. Lett.* **96**, 047207 (2006).
 - [16] F. Kruger, U. Karahasanovic, and A. G. Green, *Phys. Rev. Lett.* **108**, 067003 (2012).
 - [17] V. V. Glushkov, I. I. Lobanova, V. Yu. Ivanov, V. V. Voronov, V. A. Dyadkin, N. M. Chubova, S. V. Grigoriev, and S. V. Demishev, *Phys. Rev. Lett.* **115**, 256601 (2015).
 - [18] Y. Ishikawa, G. Shirane, J. A. Tarvin, and M. Kohgi, *Phys. Rev. B* **16**, 4956 (1977).
 - [19] J. A. Tarvin, G. Shirane, Y. Endoh, and Y. Ishikawa, *Phys. Rev. B* **18**, 4815 (1978).
 - [20] F. Semadeni, P. Boni, Y. Endoh, B. Roessli, and G. Shirane, *Physica B (Amsterdam)* **267-268**, 248 (1999).
 - [21] S. V. Demishev, I. I. Lobanova, V. V. Glushkov, T. V. Ischenko, N. E. Sluchanko, V. A. Dyadkin, N. M. Potapova, and S. V. Grigoriev, *JETP Lett.* **103**, 321 (2016).
 - [22] S. V. Grigoriev, S. V. Maleyev, E. V. Moskvina, V. A. Dyadkin, P. Fouquet, and H. Eckerlebe, *Phys. Rev. B* **81**, 144413 (2010).
 - [23] M. Janoschek, M. Garst, A. Bauer, P. Krautscheid, R. Georgii, P. Böni, and C. Pfleiderer, *Phys. Rev. B* **87**, 134407 (2013).

- [24] S. V. Grigoriev, S. V. Maleyev, A. I. Okorokov, Y. O. Chetverikov, R. Georgii, P. Böni, D. Lamago, H. Eckerlebe, and K. Pranzas, *Phys. Rev. B* **72**, 134420 (2005).
- [25] S. A. Brazovskii, I. E. Dzyaloshinskii, and B. G. Kukhareno, *Zh. Eksp. Teor. Fiz.* **70**, 2257 (1976) [*Sov. Phys. JETP* **43**, 1178 (1976)].
- [26] The data reduction software used is Graphical Reduction and Analysis SANS Program (GRASP), www.ill.eu/instruments-support/instruments-groups/groups/lss/grasp/.
- [27] A. A. Povzner, A. G. Volkov, and T. A. Nogovitsyna, *Phys. Solid State* **59**, 217 (2017).
- [28] A. A. Povzner, A. G. Volkov, and T. A. Nogovitsyna, *Phys. Solid State* **59**, 1285 (2017).
- [29] S. M. Stishov, A. E. Petrova, S. Khasanov, G. Kh. Panova, A. A. Shikov, J. C. Lashley, D. Wu, and T. A. Lograsso, *Phys. Rev. B* **76**, 052405 (2007).
- [30] S. M. Stishov and A. E. Perova, *Phys. Usp.* **54**, 1117 (2011).